AIAA 2004-0793

Direct Calculation of Spherical Detonation Initiation of a H2/O2/Ar Mixture by the CESE Method

Bao Wang and S.-T. John Yu
Ohio State University
Columbus, OH

42nd AIAA Aerospace Sciences Meeting & Exhibit
5 - 8 January 2004
Reno, Nevada

For permission to copy or to republish, contact the copyright owner named on the first page.
For AIAA-held copyright, write to AIAA Permissions Department,
1801 Alexander Bell Drive, Suite 500, Reston, VA, 20191-4344.

Direct Calculation of Spherical Detonation Initiation of $H_2/O_2/Ar$ Mixtures by the CESE Method

Bao Wang[1] and S.-T. John Yu[2]
Department of Mechanical Engineering
Ohio State University
Columbus, OH 43202

ABSTRACT

This paper reports high-fidelity simulation of the direct initiation process of spherical detonation waves by depositing various amounts of concentrated energy at the center of the explosion. The goal is to understand the underpinning mechanisms of failed or successful detonation initiation processes. One-dimensional reactive Euler equations including multiple species are solved by the Space-Time Conservation Element and Solution Element (CESE) method. Chemical reactions of $H_2/O_2/Ar$ gas mixtures are modeled by a finite-rate model composed of 9 species and 24 reaction steps. Comprehensive thermodynamics model based on the use of polynomial expression of Cp(T) of each species is employed to calculate the thermodynamic states of the reactive mixtures. Detailed results of sub-critical, critical, and supercritical initiation process, corresponding to the failed, marginally successful, and successful detonation initiation, are presented. Data analysis based on tracking the temperature of fluid particles in the reaction zone is performed. Contribution of competing terms in the equation has been analyzed. We found that the unsteadiness in the temperature reaction zone equation dominates the initiation process.

Key words: detonation initiation, critical energy, and the CESE method.

1. INTRODUCTION

In the process of direct detonation initiation [1, 2], a large amount of energy is instantaneously deposited to a small region in the middle of an unconfined combustible mixture. Immediately, a strong spherical blast wave is generated. In the radial direction, the shock wave expands and decays, while it continues heating the gas mixture. Due to shock heating, chemical reactions occur behind the shock wave and chemical energy is released. Under suitable conditions, detonation is initiated. Zeldovich et al. [1] studied the direct detonation initiation process by imposing a spark. They found that the amount of the deposited energy is the key parameter controlling the initiation process. Many attempts have been made to predict the critical energy for initiating detonation under various circumstances. Kailasanth and E. S. Oran [3] successfully developed a theoretical model to determine the relation between the power and the energy required for detonation initiation in a gas mixture by Flux-Corrected Transport (FCT) algorithm. The model shows that the power and energy are proportional to higher powers of the critic time for energy deposition. He and Clavin [4, 5] performed CFD analysis of the direct initiation process. They developed the critical curvature model, which states that the failure mechanism of the detonation is mainly caused by the nonlinear curvature effect of the wave front. Eckett et al. [6] proposed the critical decay rate model, in which they pointed out that the critical mechanism of a failed detonation initiation is due to the unsteadiness of the reacting flow. Their theory for spherical detonation initiation has been supported by numerical simulation and experimental data.

To date, numerical analyses for the detonation initiation have been based on the use of (i) single-step irreversible reaction model, and (ii) the assumption of a polytropic gas mixture. However, in a recent numerical study, Mazaheri [7] showed that with a single-step model, a decaying blast wave could unrealistically become a successful detonation in its development even when the deposited energy is well in the subcritical regime. In order to catch the essential features of real detonation initiation phenomena, Lee and Higgins [8] strongly suggested that one should abandon the single-step chemistry model and adopt real finite rate chemistry models and real thermodynamics calculations. Recently, Im and Yu

[1] Ph.D. Student, Email: wang.909@osu.edu
[2] Associate Professor, AIAA Member, Email: yu.274@osu.edu

[9] have successfully applied the CESE method to simulate the direct initiation processes of cylindrical detonations using realistic finite-rate model and thermodynamics calculations. They showed that the unsteadiness of the reacting flow is the key for the success and failure of the detonation initiation processes.

In the present work, we extend the work in [9] to spherical detonation in an $H_2/O_2/Ar$ gas mixture. A finite-rate model of twenty-four reaction steps and nine species is adopted. Similar to that in [6, 9], we analyze the temperature evolution of fluid particles in the reaction zone to study the underpinning physics in the initiation processes. In particular, we have carefully derived the temperature reaction zone equation for the reactive gas mixture without evoking any unnecessary assumptions. The derivation procedure is consistent with the comprehensive chemistry and thermodynamics models employed in the present numerical model.

The rest of the paper is organized as follows. Section 2 shows the model equations. In Section 3, we drive the reaction zone temperature equation, which will be used for data analyses to understand reaction zone evolution in the initiation process. In Section 4, we present results and discussions. We then offer concluding remarks and provide the cited references.

2. MODEL EQUATIONS

2.1 Governing Equations

We consider one-dimensional reactive Euler equations of N_s species:

$$\frac{\partial \mathbf{U}}{\partial t}+\frac{\partial \mathbf{F}(\mathbf{U})}{\partial r}=\mathbf{G}(\mathbf{U})+\mathbf{S}(\mathbf{U}), \qquad (1)$$

where

$$\mathbf{U}=(\rho,\rho u,\rho E,\rho_1,\rho_2,...,\rho_{N_s-1})^{\mathrm{T}},$$

$$\mathbf{F}=(\rho u,\rho u^2+p,(\rho E+p)u,\rho_1 u,\rho_2 u,...,\rho_{N_s-1}u)^{\mathbf{T}}$$

$$\mathbf{G}=-\frac{j}{r}\left(\rho u,\rho u^2,(\rho E+p)u,\rho_1 u,\rho_2,...,\rho_{N_s-1}u\right)^{\mathbf{T}}$$

$$\mathbf{S}=\left(0,0,0,\dot{\omega}_1,\dot{\omega}_2,...,\dot{\omega}_{N_s-1}\right)^{\mathbf{T}} \qquad (2)$$

and ρ, u, p, and E, are density, velocity, pressure and specific total energy of the gas mixture, respectively. In Eq. 2, the index $j = 0, 1,$ and 2 for planar, cylindrical, and spherical flows, respectively. ρ_k is the density of species k. ρ is the summation of all species density, i.e.,

$$\rho=\sum_{k=1}^{Ns}\rho_k \quad . \qquad (3)$$

The total energy E is defined as

$$E=e+u^2/2, \qquad (4)$$

with e the specific internal energy of the gas mixture, which is calculated based on mass-weighted average of the specific internal energy of each species e_k, i.e.,

$$e=\sum_{k=1}^{Ns}y_k e_k \qquad (5)$$

In Eq. (5), $y_k=\rho_k/\rho$ is the mass fraction of species k. Since the internal energy e and the total energy E include the heat of formation of each species, no source term exists in the energy equation. In the species equations, however, the source term $\dot{\omega}_k$ is the net mass production rate of species k.

2.2 Initial and Boundary conditions

The initial conditions are taken from reference [5]. A specific amount of energy, E_s, in the form of high temperature and high pressure (with a subscript s) is deposited instantaneously into the driver section of a reactive gas mixture. Outside of the energy deposition area, low temperature and pressure are set as the driven section.

$$\begin{aligned}\text{If } 0\le r<r_s,\quad & p=p_s, T=T_s, y_i=y_s, u=u_s,\\ r\ge r_s,\quad & p=p_0, T=T_0, y_i=y_{i0}, u=u_0\end{aligned} \qquad (6)$$

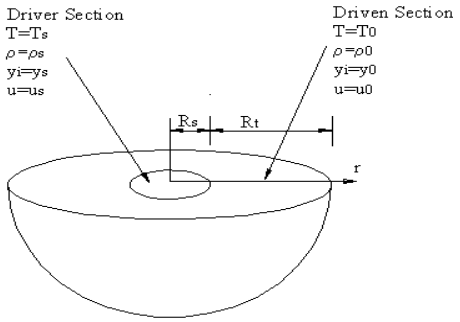

Fig. 1: A schematic of the initial condition of the direct detonation initiation process

Refer to Fig.1. The initial condition provides a strong cylindrical expanding blast wave to be expanded in the radial direction. The species compositions at both sides are H_2+O_2+7Ar. The pressure and temperature of the driven section are 0.2 atm and 298K, respectively. The deposited energy E_s is calculated based on the internal energy for a perfect gas:

$$E_s = \sigma_j r_s^{j+1} p_s /(\gamma - 1)$$
$$\sigma_j = [2j\pi + (j-1)(j-2)]/(j+1) \quad (7)$$

Therefore, the amount of the deposited energy is determined by the value of the specified pressure in the driver section. Pressure at the driver section, p_s, is set *200* atm for all calculations. Two boundary conditions are used in the calculation. At *r=0,* the singular center point condition is constructed by imposing flux balance in the setting of the CESE method. At *r=∞,* the standard CESE non-reflective boundary condition treatment is employed.

3. REACTION ZONE EUQATION

Based on Eq.1, we derive the following non-conservative form equations:

$$\frac{D\rho}{Dt} + \rho\frac{\partial u}{\partial r} + \frac{j}{r}\rho u = 0 \quad (8)$$

$$\frac{Du}{Dt} + \frac{1}{\rho}\frac{\partial p}{\partial r} = 0 \quad (9)$$

$$\frac{De}{Dt} - \frac{P}{\rho^2}\frac{D\rho}{Dt} = 0 \quad (10)$$

$$\frac{Dy_k}{Dt} = \Omega_k \quad (11)$$

Here we used $\dot{\omega}_k = \rho\Omega_k$. Notice that $v = \frac{1}{\rho}$ is the specific volume of the gas mixture. Equation 10 can be written as

$$\frac{De}{Dt} + P\frac{Dv}{Dt} = 0 \quad (12)$$

To proceed, we eliminate $\frac{De}{Dt}$ from Eq. (12) by using the differential relation for the equation of state $e(P, \rho, y_1, y_2, ..., y_N)$,

$$de = \left(\frac{\partial e}{\partial P}\right)_{v,y_1,y_2,...y_N} dP + \left(\frac{\partial e}{\partial v}\right)_{P,y_1,y_2,...y_N} dv + \sum_1^N \left(\frac{\partial e}{\partial y_k}\right)_{P,v,y_1,y_2,...y_N,j\neq k} dy_k \quad (13)$$

$$\frac{DP}{Dt} = \frac{\left(\frac{De}{Dt} - \left(\frac{\partial e}{\partial v}\right)_{P,y_1,y_2,...,y_N}\frac{Dv}{Dt} - \sum_1^N \left(\frac{\partial e}{\partial y_k}\right)_{P,v,y_1,y_2,...,y_N,j\neq k}\frac{Dy_k}{Dt}\right)}{\left(\frac{\partial e}{\partial P}\right)_{v,y_1,y_2,...y_N}} \quad (14)$$

Substitute Eq. (12) into Eq. (14), we have

$$\frac{DP}{Dt} = -\frac{\left(P + \left(\frac{\partial e}{\partial v}\right)_{P,y_1,y_2,...y_N}\right)}{\left(\frac{\partial e}{\partial P}\right)_{v,y_1,y_2,...y_N}} v^2\rho^2\frac{Dv}{Dt} - \sum_1^N \frac{\left(\frac{\partial e}{\partial y_k}\right)_{P,v,y_1,y_2,...,y_N,j\neq k}}{\left(\frac{\partial e}{\partial P}\right)_{v,y_1,y_2,...y_N}}\frac{Dy_k}{Dt} \quad (15)$$

With $c^2 = \frac{\left(P + \left(\frac{\partial e}{\partial v}\right)_{P,y_1,y_2,...,y_N}\right)}{\left(\frac{\partial e}{\partial P}\right)_{v,y_1,y_2,...,y_N}} v^2$ and

σ_k is the thermicity coefficient of the species k, given by

$$\sigma_k = \frac{1}{\rho c^2}\left(\frac{\partial P}{\partial y_k}\right)_{e,v,y_1,y_2,...,y_{N,j\neq k}} = -\frac{1}{\rho c^2}\frac{\left(\frac{\partial e}{\partial y_k}\right)_{P,v,y_1,y_2,...,y_N,j\neq k}}{\left(\frac{\partial e}{\partial P}\right)_{v,y_1,y_2,...,y_N}} \quad (16)$$

Eq. (15) can be written as

$$\frac{DP}{Dt} = -\rho^2 c^2\frac{Dv}{Dt} + \rho c^2\sum_1^N \sigma_k\frac{Dy_k}{Dt} \quad (17)$$

By using Eq.(11), we have

$$\frac{DP}{Dt} = -\rho^2 c^2\frac{Dv}{Dt} + \rho c^2\sum_1^N \sigma_k\Omega_k \quad (18)$$

Note that $v = \frac{1}{\rho}$ and $\frac{Dv}{Dt} = -\frac{1}{\rho^2}\frac{D\rho}{Dt}$, and we have

$$\frac{DP}{Dt} = c^2\frac{D\rho}{Dt} + \rho c^2\sum_1^N \sigma_k\Omega_k \quad (19)$$

Consider another form of the energy equation

$$\frac{DP}{Dt} = c^2\frac{D\rho}{Dt} + \rho c^2\dot{\sigma} \quad (20)$$

where c is the frozen sound speed and $\dot{\sigma} = \sum_{1}^{N} \sigma_k \Omega_k$ is the total thermicity summing over all species.

To obtain the reaction zone equations, using the following transformation:

$$x = R(t) - r$$

$$w(x,t) = U(t) - u(r,t)$$

where R and U are the position and velocity of the shock in the fixed reference frame, respectively. To recap, the above equation of motion can be written as

$$\frac{D\rho}{Dt} + \rho\frac{\partial w}{\partial x} + \frac{j}{R-x}\rho(U-w) = 0 \quad (21)$$

$$\frac{Dw}{Dt} + \frac{1}{\rho}\frac{\partial p}{\partial r} = \frac{DU}{Dt} \quad (22)$$

$$\frac{DP}{Dt} = c^2\frac{D\rho}{Dt} + \rho c^2\dot{\sigma} \quad (23)$$

$$\frac{Dy_k}{Dt} = \Omega_k \quad (24)$$

Equations 21 and 22 can be written as

$$\frac{D\rho}{Dt} = -\frac{\rho}{w}\frac{Dw}{Dt} + \frac{\rho}{w}\frac{\partial w}{\partial t} - \frac{j}{R-x}\rho(U-w) \quad (25)$$

$$\frac{DP}{Dt} = -\rho w\frac{Dw}{Dt} + \frac{\partial P}{\partial t} + \rho w\frac{DU}{Dt} \quad (26)$$

Substituting Eqs. (25-26) into Eq. (22) gives

$$\eta\frac{Dw}{Dt} = w\dot{\sigma} - \frac{j}{R-x}w(U-w) + \frac{\partial w}{\partial t} + \frac{\partial w}{\partial t} - \frac{w}{\rho c^2}\frac{\partial p}{\partial t} - M^2\frac{DU}{Dt} \quad (27)$$

Substituting Eq. (27) into Eqs. (25-26) gives

$$\eta\frac{D\rho}{Dt} = -\rho\dot{\sigma} - \frac{j}{R-x}\rho M^2(U-w) - \frac{\rho w}{c^2}\frac{\partial w}{\partial t} + \frac{1}{c^2}\frac{\partial p}{\partial t} + \frac{\rho w}{c^2}\frac{DU}{Dt} \quad (28)$$

$$\eta\frac{DP}{Dt} = -\rho w^2\dot{\sigma} + \frac{j}{R-x}\rho w^2(U-w) - \rho w\frac{\partial w}{\partial t} + \frac{\partial p}{\partial t} + \rho w\frac{DU}{Dt} \quad (29)$$

Here the Mach number *Ma* and sonic parameter η are given by $Ma = \frac{w}{c}$, $\eta = 1 - Ma^2$.

Equations (27- 29) are the solutions for the velocity, density and pressure gradients along a Lagrangian particle behind the leading shock wave of a traveling detonation. They are referred as reaction zone equations by Eckett et al. [6]. In each equation, the first term on the right-hand side is due to the contribution from the chemical heat release, the second tem is due to wave curvature, and the remaining terms are from unsteadiness of the flow.

Considering an idea gas

$$P = \rho RT \quad (30)$$

Where *T* is the temperature and *R* is the gas constant of the gas mixture, which is given by

$$R = \frac{R_u}{M} = R_u\sum\frac{y_k}{M_k} \quad (31)$$

Where R_u is the universal gas constant, *M* is the mean molar weight of the gas mixture and M_k is the molar weight of the species *k*. The frozen sound speed is given by

$$c = \left(\frac{\gamma P}{\rho}\right)^{1/2} \quad (32)$$

Where γ is the ratio of the specific heats of the gas mixture? To proceed, we derive the temperature gradient equation. Taking the substantial derivative of Eq. (30),

$$\frac{DP}{Dt} = \frac{P}{\rho}\frac{D\rho}{Dt} + \frac{P}{T}\frac{DT}{Dt} \quad (33)$$

Aided by Eqs. (29) and (32), Eq. (33) can be rewritten as

$$\rho R\eta\frac{DT}{Dt} = \eta\frac{DP}{Dt} - \frac{c^2}{\gamma}\eta\frac{D\rho}{Dt} \quad (34)$$

Substituting Eqs. (28) and (29) into Eq. (34), and using $C_p = \frac{\gamma R}{\gamma - 1}$, we have

$$\eta C_p\frac{DT}{Dt} = \frac{\gamma}{\gamma-1}\left(\frac{c^2}{\gamma} - w^2\right)\dot{\sigma} + \frac{j}{R-x}w^2(U-w) - w\frac{\partial w}{\partial t} + \frac{1}{\rho}\frac{\partial p}{\partial t} + w\frac{DU}{Dt} \quad (35)$$

Aided by

$$\sigma_k = \frac{1}{\gamma}\left(\frac{M}{M_k} - \frac{e_k}{C_v T}\right) \tag{36}$$

and the definition of the total thermicity

$$\dot{\sigma} = \sum_1^N \sigma_k \Omega_k$$

we have

$$\eta C_p \frac{DT}{Dt} = -\left(1 - \gamma Ma^2\right)\sum_{i=1}^{N} e_i \Omega_i - \frac{c^2}{\gamma}\sum_{i=1}^{N}\frac{M}{M_i}\Omega_i + \frac{j}{R-x}w^2(U-w) - w\frac{\partial w}{\partial t} + \frac{1}{\rho}\frac{\partial p}{\partial t} + w\frac{DU}{Dt} \tag{37}$$

When the detonation wave propagates into the reactant mixture, a sharp temperature increase occurs. If the flow particles are quickly ignited by the temperature rises due to shock heating, the detonation will be sustained. Because chemical reaction rate depends on the temperature of the flow particles. Evolving temperature profiles in the reaction zone provide the most valuable information about failure or success of the detonation initiation process.

The left-hand side of Eq. (37) is the substantial derivative of fluid particle temperature. The first term on the right-hand side is the chemical heat release term, the second term is due to the curvature effect, and the remaining terms are the unsteadiness terms. Note that with only heat release term on the right hand side, Eq. (37) is for a planar detonation wave at a stationary state.

In the setting of the simplified thermal-chemical model equations, Eckett et al. [6] compared the magnitude of each term in Eq. (37) to determine the physics of the detonation initiation process. In this paper, we conduct similar studies based on numerical results obtained by employing realistic finite-rate chemistry and thermodynamics models. The goal here is to identify the dominant effect among the competing terms in Eq. (37) via tracking fluid particles in the reaction zone of an evolving detonation wave.

5. RESULTS AND DISCUSSION

Bach, Knystautas, and Lee [2] proposed that three propagation regimes exist in the direct detonation initiation process, i.e., the sub-critical, the critical, and the supercritical regimes. In the sub-critical regime, the deposited initiation energy is below a critical value, the reaction front would decouple from the leading shock wave as time evolves. As a result, the detonation decays to a shock wave and then later a acoustic wave; detonation would fail. In the critical regime, the deposited energy is very close to a critical value for a sustainable detonation wave initiation. At the initial stage of the wave development, the overdriven detonation continuously decays. After a period of time, the shock wave and the reaction front propagate at a quasi-steady mode, propagating at almost constant shock velocity. Suddenly, local explosions occur at isolated spots in reaction zone, and a detonation wave is developed. The flow is highly unstable with significant pressure spikes in the initiation process. In the supercritical regime, the deposited initiation energy greatly exceeds the critical value. The shock wave is always attached to the reaction front. The overdriven detonation decays and asymptotically approaches a self–sustained CJ detonation.

We consider 6 values of Es: 1950J, 3510J, 3542J, 5220J, 7650J, and 8650J, in which 1950J and 3510 J are in the subcritical regime, and 8650J is in the super critical regime, and the rest are in the critical regime, where we expect significant flow instabilities. Figure 2 shows the pressure histories of each about case. The ratio of local maximum pressure to initial reactant pressure is plotted as a function of the radial locations of the leading shock wave. For reference, the pressure of the von-Neuman spike of the corresponding self sustained CJ detonation (for the driven section) is also plotted by a dot line. In a series of calculations by incrementally increasing the values of the deposited initiation energy, we can clearly observe the three regimes [2].

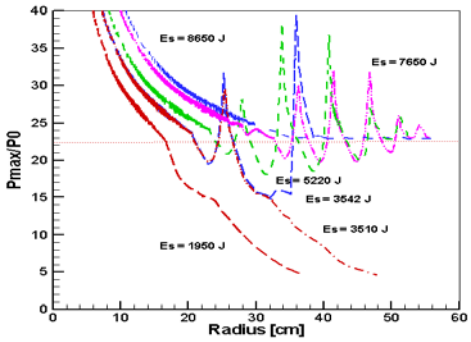

Fig. 2: The spatial histories of local maximum pressures in the three regimes of direct initiation processes of a spherical detonation in a $H_2 + O_2 + 7Ar$ mixture.

When the initial energy E_s = 1950.0 *J*, the strong blast wave decays to a wave with peak pressures much lower than the von Neumann value, indicating a failed initiation process. When the initial energy Es is 2000~3510 *J*, a pressure peak occurs at the initial stage of the initiation process. However, the

detonation process would ultimately fail as time evolves. .

Three initial energies of $E_s = 3542\ J$, $E_s = 5220\ J$ and $E_s = 7650\ J$ are in the critical regime. Distinct pressure peaks are observed. The deposited initiation energies are not high enough to achieve stable detonation waves quickly. In all cases, the unstable period ends around $R = 55\ cm$, and the waves become a self–sustained CJ detonation wave. There is wide range of the deposited Es that the initiation processes show significant instability waves. Based on the calculations, the minimum critical Es is about 3540 J. With higher initiation energy in the super-critical regime, e.g., $E_s = 8650\ J$, the initial blast wave directly initiate the detonation wave, which expands and decays to the CJ value with mild instabilities.

In the rest of the discussions, we have focused on detailed analyses of two cases: Es = 1950J, a failed process, and Es = 7650J, a successful process in the critical regime. Figure 3 shows the time histories of pressure profiles for Es = 1950J. Initially, strong pressure wave continuously decays to be below the von Neumann pressure. At $R = 24\ cm$ (pressure profile marked by red ink), the shock wave is decoupled from the reaction front and the detonation initiation fails.

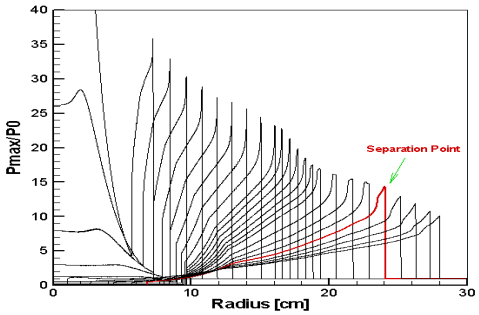

. Fig. 3: Spatial pressure profile for the failed initiation process. $E_s = 1950\ J$.

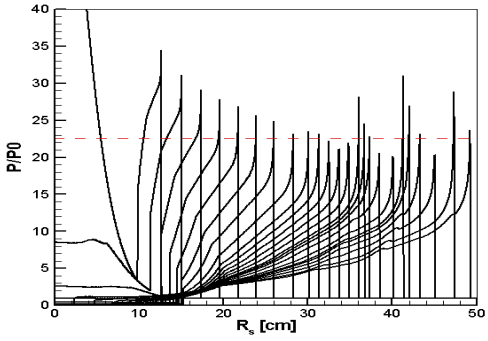

Fig. 4: Spatial pressure profile for the critical initiation process. $E_s = 7650\ J$.

In Fig.4, Es = 7650J. The initial development of the reactive wave is similar to that of Fig.3. However, at $R = 32.8\ cm$, pressure pulse occurs, and the reactive wave becomes unstable. Intermittently, overdriven detonation waves occur and the pressure peaks of this overdriven detonation wave rise above the von Neumann pressures. As time evolves, it gradually converges to the CJ detonation, indicating a successful initiation process. Note that this galloping type of pressure waves could also be observed in simulation using simplified model equations based on the use of polytropic gas and one-step irreversible reaction.

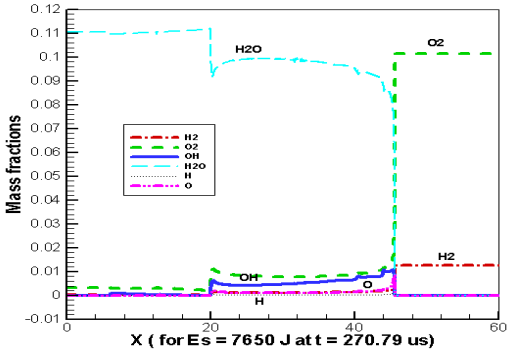

Fig. 5: Snapshot of species mass fractions at time t = 192.3 μs for Es = 7650 J, a successful detonation initiation process.

Figure 5 shows mass fractions of chemical species at time $t = 192.3\ \mu s$ for the case of Es=7650 J. Species composition changes rapidly inside the reaction zone. In the present calculation, the reaction zone is determined by the mass fraction of H_2O since it varies from 0 to a maximum value in the reaction zone. We specify that the reaction zone is the region that 95% > [H_2O] > 5%.

Figure 6 shows velocity profiles at different times for a successful initiation process with $E_s = 7650\ J$. At the later stage of flow development, the low pressure at the center of the explosion would draw the fluid inward, and for a backward shockwave. When the backward shockwave moves close to the center of the domain, the shock velocity increases extremely quickly until it hits the center point and then reflects back to expand outwardly.

The position of the leading shock, the locations of 5% and 95% mass fraction of H_2O are plotted against the elapsed time in Figs. 7 and8 for Es =1950 J and 7650 J, respectively, to show the development of the reaction zone. In Fig. 7, when shock is strong at the initial stage, the reaction zone is attached to the shock wave. At around $R = 24\ cm$, however, the reaction zone begins to detach from the shock wave, indicating that the detonation has failed. In Fig.8, the reaction

front is continuously coupled with the shock wave, indicating successful initiation of a detonation wave.

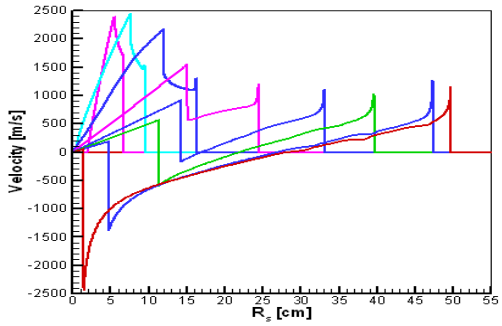

Fig. 6 Velocity profiles for E_s = *7650 J* at the different times.

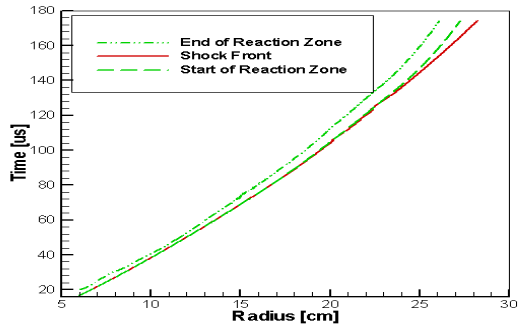

Fig. 7: Evolving reaction zone versus time for Es = 1950 J, a failed initiation processes

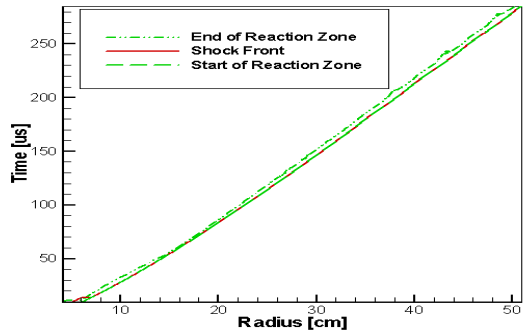

Fig. 8: Evolving reaction zone versus time for Es = 7650 J, a successful initiation process

In the critical regime, e.g., E_s = *3510 J* and E_s = *3542 J*, there exist a critical point in the space-time domain such that failure or success of the initiation process is determined. This critical point always occurs before the formation of pressure pulses that indicate the re-acceleration of the decaying shock. Instead of the address of re-accelerating mechanism, Eckett et al. [6] proposed to compare the magnitude of various terms in the temperature reaction zone equation to understand the failed initiation process. To follow this approach, we use the temperature reaction zone equation to extract the Lagrangian particle path data from the CFD solution.

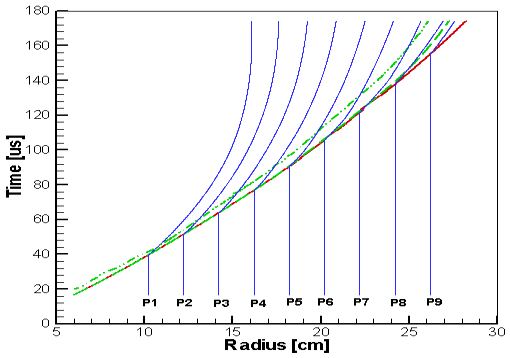

Fig. 9 Particle trajectories for the case of Es = 1950 J, in a failed initiation process

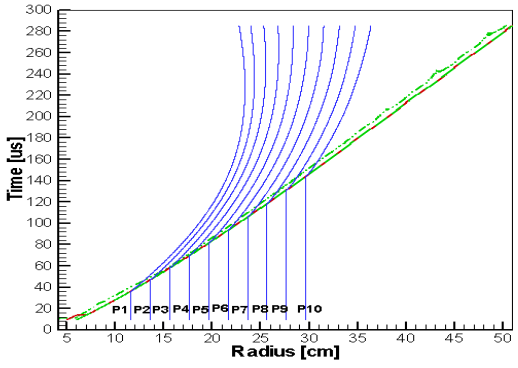

Fig. 10 Particle paths for Es = 7650 J, in a successful initiation process

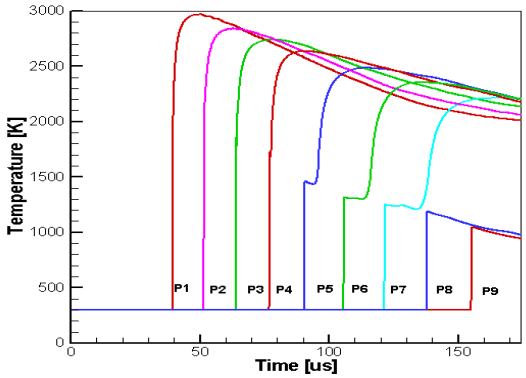

Fig. 11: Temperature histories of fluid particle paths for E_s = *1950 J*.

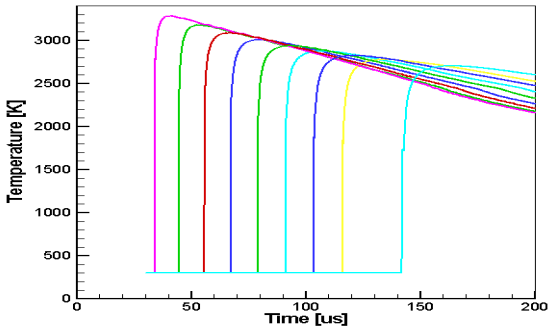

12. Fig. 12: Temperature histories of fluid particle paths for $E_s = 7650\ J$.

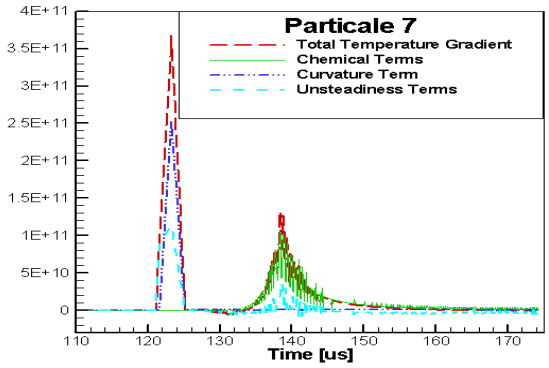

Fig. 13: Competing unsteadiness terms along the particle path 7 for Es = 1950 J.

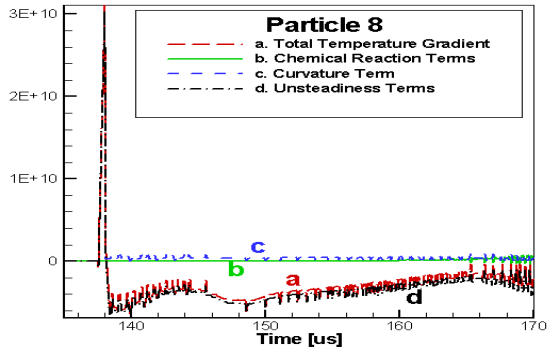

Fig. 14: Competing unsteadiness terms of the particle 8 for Es = 1950 J.

For the case Es = 1950 J, Fig. 9 shows the paths of particles that cross the leading shock around the time of detonation failure. Figure 11 shows the temperature profiles of the fluid particles as a function of time. . After about 140 μs, the earlier fluid particle paths show deceleration and moving back towards the origin. For comparison, similar results of a successful initiation process are given in Fig. 10 and Fig. 12.

The temperature profiles are also similar to those in [6, 9]. In the failed process, the earlier particles are rapidly heated up by the chemical reactions. However, for the fifth to seventh particles, the ignition delays have significantly increased. The last two particles never heat up because the blast wave becomes too weak to ignite the reactant.

To examine the competing terms in the temperature reaction zone structure equation, Eq. (37), we rewrite the equation for the spherical coordinate ($j = 2$) into the following form:

$$\underbrace{\eta C_p \frac{DT}{Dt}}_{\text{Total}} = \underbrace{-(1-\gamma M^2)\sum e_k \Omega_k - \frac{c^2}{\gamma}\sum \frac{W}{W_k}\Omega_k}_{\text{Heat release}} + \underbrace{\frac{2}{R-x}w^2(U-w)}_{\text{Curvature}} + \underbrace{w\frac{dU}{dt} - w\frac{\partial w}{\partial t} + \frac{1}{\rho}\frac{\partial P}{\partial t}}_{\text{Unsteadiness}} \quad (38)$$

Figure 13 shows magnitudes of each term in Eq. (38) along the particle trajectory at Particle 7, a particle with successful chemical reactions in the initiation process. When shock front comes to the initial position of Particle 7, there is a sharp increase of the time derivative of temperature. After the shock front pasts the particle, the time derivative temperature decreases very quickly, but temperature continue increasing until it reaches 1250 K. This process takes about 4 μs. After that temperature decreases slightly. It is interesting to note that after an increased explosion time of about 9 μs, chemical reactions take place and there come another temperature increase due to the chemical ignition. After chemical reactions complete, the time derivative of temperature (Fig.13) diminishes and temperature decreases (Fig. 11) slowly.

For Es= 1950 J and Particle 8, Fig. 14 shows magnitudes of each term in the temperature reaction zone equation, Eq. (38), along the particle trajectory at a failure point of the initiation process. The present results show that the effect of the curvature term contributes little to the time derivative of temperature as compared to other terms. On the other hand, the

effect of the unsteadiness term is significant during the course of failed initiation process.

6. CONCLUDING REMARKS

Numerical simulations of the direct initiation processes of spherical detonations in a H_2-O_2-Ar mixture have been conducted using the CESE method with realistic finite-rate chemistry models and comprehensive thermodynamics calculations. The three detonation initiation regimes were calculated according to the values of the deposited energy in the initial conditions, including sub-critical, critical, and supercritical. In the critical regime, the present result showed flow instabilities with strong pressure peaks. The magnitude of each term in the temperature reaction zone equation was calculated. The results of present study showed that the unsteadiness plays a critical role in the failure of detonation initiation.

REFERENCES

1. I. B. Zel'dovich, S. M. Kogarko, and N. N. Simonov, (1956), "An experimental investigation of spherical detonation of gases," Sov. Phys. Tech. Phys. 1(8), pp. 1689-1713.
2. G. G. Bach, R. Knystautas, and J. H. Lee, (1969), "Direct Initiation of Spherical Detonations in Gaseous Explosives," 12th Symp. Int. Combust. Proc., pp. 853-867.K. Kailasanath, E. S. Oran, *Prog. in Astro. and Aero.* 94 (1985) 38-54.
3. L. He and P. Clavin, (1994), "On the Direct Initiation of Gaseous Detonations by an Energy Source," J. Fluid Mech. 277, pp. 227-248.
4. L. He, (1996), "Theoretical Determination of the Critical Conditions for the Direct Initiation of Detonation in Hydrogen-Oxygen Mixtures," Combustion and Flame 104, pp. 401-418.C. A. Eckett, J. J. Quirk, and J. E. Shepherd, J. Fluid Mech. 421(2000) 147-183.
5. K. Mazaheri, (1997), "Mechanism of the onset of detonation in blast initiation," PhD thesis, McGill University.
6. J. H. S. Lee and A. J. Higgins, (1999), "Comments on Criteria for Direct Initiation of Detonation," Phil. Trans. R. Soc. Lond., A 357, pp3503-3521.
7. Kyoung-Su Im, S.-T. John Yu, "Analyses of Direct Detonation Initiation with Realistic Finite-Rate Chemistry", AIAA-2003-1318 the 41th Aerospace Sciences Meeting and Exhibit, January 2003, Reno, NV.K.
8. K.-S. Im, C.-K. Kim, and S.-T. J. Yu, "Application of the CESE Method to Detonation with Realistic Finite-Rate Chemistry," AIAA-2002-1020 the 40th Aerospace Sciences Meeting and Exhibit, January 2002, Reno, NV.
9. S. T. Yu, S. C., Chang, P. C. E. Jorgenson, "Direct Calculation of Detonation with Multi-Step Finite-Rate Chemistry by the Space-Time Conservation Element and Solution Element Method," AIAA Paper 99-3772, AIAA 30th Fluid Dynamics Conference and Exhibit, June 1999, Norfolk, VA.